# Long-range ferromagnetic ordering in manganese-doped two-dimensional dichalcogenides

Rohan Mishra,[1,2,*] Wu Zhou,[2] Stephen J. Pennycook,[2] Sokrates T. Pantelides,[1,2] and Juan-Carlos Idrobo[2]

[1]*Department of Physics and Astronomy, Vanderbilt University, Nashville, Tennessee 37235, USA*

[2]*Materials Science and Technology Division, Oak Ridge National Laboratory, Oak Ridge, Tennessee 37831, USA*

(Received 2 April 2013; revised manuscript received 12 August 2013; published 10 October 2013)

We report an investigation of long-range ferromagnetic (FM) ordering in Mn-doped $MoS_2$, $MoSe_2$, $MoTe_2$, and $WS_2$ for Mn concentration less than 5% using density functional theory calculations. The long-range ferromagnetism of Mn spins is mediated by an antiferromagnetic (AFM) exchange between the localized Mn *d* states and the delocalized *p* states of the S, Se, and Te atoms. In contrast, transition metals like Fe, Co, and Ni show a FM exchange with the S, Se, and Te atoms, which results in a very weak FM (even slightly AFM) coupling for transition-metal defects with large separations. The Mn substitution at Mo or W sites is energetically favorable, thus making the Mn-doped dichalcogenides promising candidates for two-dimensional dilute magnetic semiconductors.

DOI: 10.1103/PhysRevB.88.144409 PACS number(s): 75.50.Pp, 75.30.Hx

Spintronics is an emerging technology based on devices that can process and store information by exploiting both the charge and the spin degree-of-freedom of electrons. Dilute magnetic semiconductors (DMS), such as Mn-doped GaAs, have been extensively studied since their discovery because they display carrier-mediated ferromagnetism, which makes them ideal for spintronics applications by offering the possibility of electronic control of magnetism.[1,2] Similarly, graphene, a two-dimensional (2D) form of carbon, has caught the attention of the materials community by providing a new platform to explore novel functionalities and even new material-based phenomena.

From the point of view of spintronics, graphene has been an excellent choice for transporting spin information over practical distances due to its long spin-diffusion distances.[3] However, a spintronics device also requires generation and detection of tunable spin currents, which can ideally be done using a ferromagnetic (FM) semiconductor. The intrinsic zero band gap of graphene along with the lack of experimental evidence for long-range ordering of defects with magnetic moment, e.g., vacancies,[4,5] limit it as a 2D DMS candidate. On the other hand, 2D transition-metal (TM) dichalcogenides, such as $MoS_2$, $MoSe_2$, $WS_2$, and others, hold promise for flexible and transparent electronics applications, owing to their sizeable band gaps within the 1–2 eV range. There have already been several reports of $MoS_2$-based transistors.[6,7] More recently, $MoS_2$ has been demonstrated as a candidate for "valleytronics," where the carrier population at the different valleys in the Brillouin zone can be controlled using a circularly polarized light.[8] FM ordering has been reported recently in TM-doped including Mn-doped $MoS_2$.[9,10]

In this paper, we report an investigation of long-range FM ordering in 2D manganese-doped molybdenum dichalcogenides and in tungsten disulfide for fairly dilute concentrations (less than 5% doping), using first-principles density functional theory (DFT). We find the presence of an antiferromagnetic (AFM) coupling between the localized Mn 3*d* states and the delocalized *p* states of the chalcogen atoms. This AFM *p-d* exchange interaction in turn drives FM ordering of localized spins of other Mn atoms and is different than the double-exchange interaction mechanism proposed in Ref. 10. The calculations also show that Mn substitution in Mo or W sites is energetically favorable, suggesting that the Mn-doped dichalcogenides are promising 2D DMS candidates. For other 3*d* TM atoms such as Fe, Co, and Ni, FM ordering is present only between nearest neighbors, as their magnetism is driven predominantly by their localized 3*d* states.

DFT calculations were performed using a plane-wave basis set with a cut-off energy of 450 eV and the projector-augmented-wave (PAW) method[11] as implemented within the Vienna *Ab initio* Simulation Package (VASP) code.[12,13] Electron exchange and correlation effects were described within the generalized gradient approximation (GGA) in the Perdew–Burke–Ernzerhof (PBE) parametrization.[14] In order to check the convergence of the results with supercell size, two supercells of size $5 \times 5 \times 1$ and $7 \times 7 \times 1$ of the $MoX_2$ primitive cell were used with a separation of 20 Å between two layers. The atomic positions were relaxed using a $2 \times 2 \times 1$ Monkhorst–Pack *k*-points mesh[15] until the forces per ion were smaller than 1 meV/Å. The electronic calculations were performed using a dense mesh with $6 \times 6 \times 1$ *k*-points.

The molybdenum dichalcogenides (MoDCs) with a chemical formula of $MoX_2$ have a layered structure, where two hexagonal planes of chalcogens (S, Se, Te) are separated by a plane of Mo atoms. $MoX_2$ layers have a $P\bar{6}m2$ space group symmetry with the Mo atoms having a trigonal prismatic coordination with the chalcogen atoms, as shown in Fig. 1. Moving down in the Periodic Table from S to Te, we find an increase in the lattice constants and a decrease in the band gaps (see Supplemental Material Table S1).[16]

Perfect MoDCs have an equal number of electrons in their up- and down-spin channels, and hence do not display any magnetic moment. With the aim to investigate if a long-range magnetic ordering can be present in the MoDCs, we substitutionally doped the Mo site with Mn atoms (labeled as $Mn_{Mo}$). The formation energy ($E_f$) of $Mn_{Mo}$ defects was defined as

$$E_f(\mathrm{Mn_{Mo}}) = E(\mathrm{Mn_{Mo}}, \mathrm{Mo_{N-1}X_{2N}}) - E(\mathrm{Mo_N X_{2N}}) - \mu_{\mathrm{Mn}} + \mu_{\mathrm{Mo}}, \quad (1)$$

 

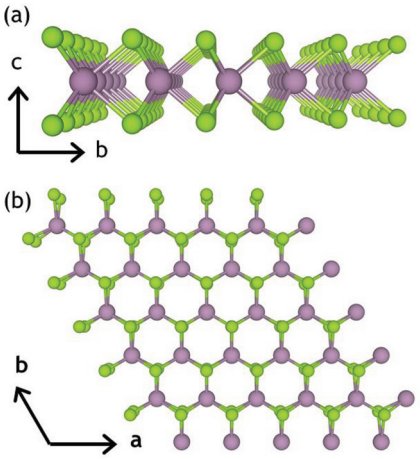


FIG. 1. (Color online) Schematic structure of $MoX_2$ monolayer (a) showing Mo atoms sandwiched between two chalcogen planes when viewed from the [100] crystallographic orientation, and (b) showing the hexagonal arrangement of Mo atoms and chalcogen atoms when viewed along the $c$ axis.

where $E(Mo_N X_{2N})$ and $E(Mn_{Mo}, Mo_{N-1} X_{2N})$ are the relaxed energies of $N$ formula units of stoichiometric $MoX_2$ and of $N$ formula units of $MoX_2$ with a single $Mn_{Mo}$ defect, respectively. $\mu_{Mn}$ and $\mu_{Mo}$ are the respective chemical potentials of a single Mn and Mo atom. We use the energy per atom of $\alpha$-Mn metal as $\mu_{Mn}$. $\mu_{Mo}$ is defined within a range of values corresponding to Mo-rich or $X$-rich growth conditions. For a Mo-rich condition, $\mu_{Mo}$ is taken as the energy of a Mo atom within its stable $fcc$ lattice, while for an $X$-rich condition, $\mu_{Mo}$ is determined from the difference in energy between a diatomic $X_2$ molecule and one formula unit of stoichiometric 2D $MoX_2$.[17]

We find that $Mn_{Mo}$ defects are energetically favorable to be created. Especially, under $X$-rich growth conditions, which favor Mo vacancies, the formation energy for creating $Mn_{Mo}$ in $MoS_2$, $MoSe_2$, and $MoTe_2$ is $-1.8$, $-0.5$, and 0 eV, respectively. We also find the formation energy of substituting Mo with other 3$d$ TM elements to be fairly small (see Supplemental Material Fig. S1),[16] which is confirmed by recent experimental reports of Co and Nb doping in $MoS_2$.[18]

Having established the stability of $Mn_{Mo}$ defects in 2D $MoX_2$, we look at the way a single $Mn_{Mo}$ changes the electronic and magnetic properties of the host $MoX_2$. We use Mn-doped $MoSe_2$ as a representative case to discuss the results since the electronic and magnetic properties of all three Mn-doped MoDCs are similar.

$Mn_{Mo}$ gives rise to highly localized states within the band gap, as shown in the density of states (DOS) plots in Figs. 2(a) and 2(b). From the orbital resolved up-spin projected DOS on the $Mn_{Mo}$ defect [Fig. 2(c)], it can be seen that the five Mn 3$d$ states split into three groups under the trigonal prismatic environment of the chalcogen atoms. The Mn $d_{xz}$ and $d_{yz}$ states are directed toward the chalcogens and hence have greater overlap with the Se 4$p$ states. Consequently, these two antibonding states ($e_2$) are degenerate and are present at

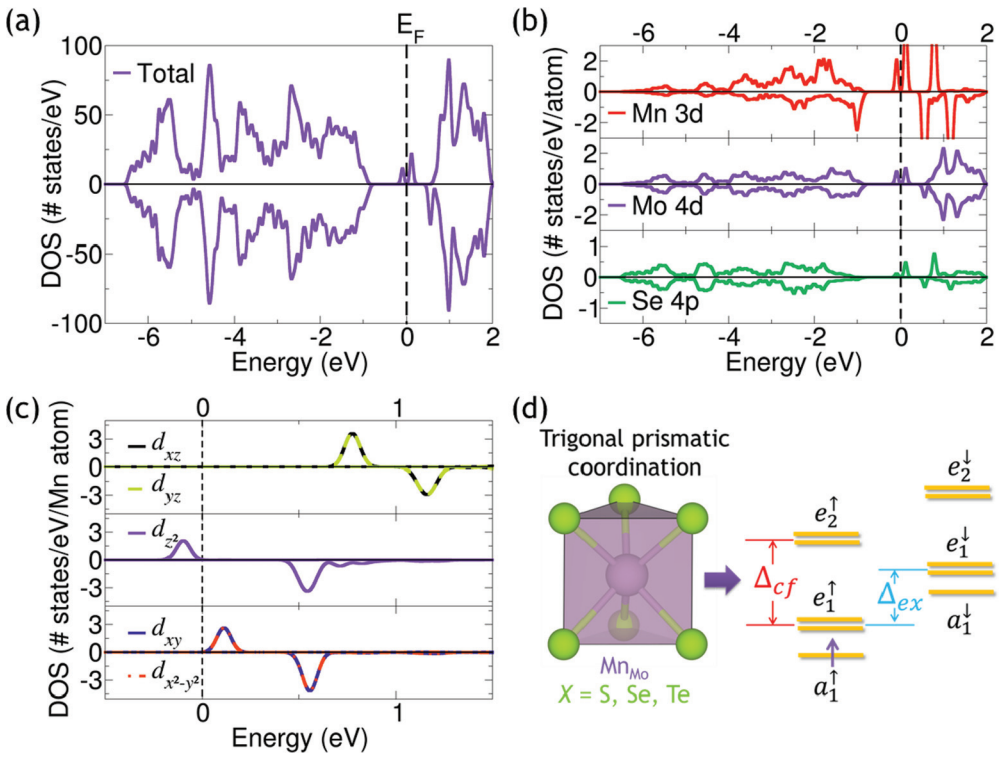


FIG. 2. (Color online) Spin resolved (a) DOS of a 75-atom supercell of $MoSe_2$ with a single $Mn_{Mo}$ defect, (b) atom-projected DOS showing the 3$d$ states of $Mn_{Mo}$ defect and 4$d$ and 4$p$ states of its neighboring Mo and Se atoms, respectively, and (c) 3$d$ states of $Mn_{Mo}$ projected onto the five different $d$ orbitals. Positive (negative) values of DOS represent up-spin (down-spin) states. All states have been normalized to the Fermi energy. (d) Schematic of the splitting of the Mn $d$ orbitals due to the trigonal prismatic coordination of the Se atoms (crystal-field splitting, $\Delta_{cf}$) and the intratomic Hund's exchange ($\Delta_{ex}$).

higher energies. On the other hand, the $d_{z^2}$ antibonding state ($a_1$) has the smallest overlap with the Se 4$p$ states due to its symmetry and therefore is the Mn 3$d$ orbital with the lowest energy. The remaining $d_{xy}$ and $d_{x^2-y^2}$ antibonding states ($e_1$) have intermediate overlap with the Se 4$p$ states and hence lie in between the $a_1$ and $e_2$ states. This kind of splitting is commonly known as crystal-field splitting ($\Delta_{cf}$). The Mn 3$d$ states also undergo an intratomic (Hund's) exchange splitting ($\Delta_{ex}$), which means the up-spin and down-spin states with the same symmetry have different energies. In the case of Mn-doped $MoSe_2$, we find that the down-spin $a_1$ and $e_1$ states are at lower energies than the up-spin $e_2$ states, which suggests that $\Delta_{ex} < \Delta_{cf}$ [as shown schematically in Fig. 2(d)]. For the case of $MoS_2$ and $MoTe_2$, although their band gaps are different, Mn substitution leads to localized states within the band gap, with only the $d_{z^2}$ state being occupied, similar to the case of $MoSe_2$, as discussed here (Supplemental Material Fig. S2).[16]

In a simple ionic scenario, the additional valence electron in Mn compared to Mo should result in only the $a_1^{\uparrow}$ state being occupied, which should result in a magnetic moment of 1 $\mu_B$ per Mn atom. However, charge sharing within the Mn, Mo, and Se atoms leads to significant differences over the simplistic ionic scenario. Integrating the DOS projected on the $Mn_{Mo}$ site gives a total of 3.18 $e$ and 1.91 $e$ for the up-spin and down-spin channels, respectively. Therefore, the total magnetic moment on the $Mn_{Mo}$ defect is $+1.27$ $\mu_B$. The integration over all the occupied Se 4$p$ states of each Se atom bonded to the $Mn_{Mo}$ defect gives a magnetic moment of $-0.03$ $\mu_B$. As there are six Se atoms around the $Mn_{Mo}$ defect, this leads to a total moment of $-0.19$ $\mu_B$. Similarly, the six Se atoms in the second nearest-neighbor position to the $Mn_{Mo}$ defect carry a total magnetic moment of $-0.04$ $\mu_B$. Summing over all the occupied 4$d$ states of the first nearest-neighbor Mo atoms does not result in any spin polarization. The distribution of spin is shown in the spin density isosurface plot in Fig. 3(a).

The above analysis tells us that hybridization between the localized Mn 3$d$ and the delocalized Se 4$p$ states leads to an AFM coupling between the Mn spins and Se spins. More importantly, every time the Se spins come across a $Mn_{Mo}$ defect, the AFM alignment between Se and Mn leads to an effective FM alignment of all the $Mn_{Mo}$ spins. Given the delocalized nature of the Se 4$p$ states, FM alignment between the $Mn_{Mo}$ spins can also be expected to act over a long range.

Indeed, the introduction of a second $Mn_{Mo}$ defect within the $MoSe_2$ supercell results in an energetically more favorable FM coupling between the defect spins than an AFM coupling. The difference in energies between FM and AFM coupling as a function of the $Mn_{Mo} - Mn_{Mo}$ distances for the Mn-doped $MoS_2$, $MoSe_2$, and $MoTe_2$ in a 75-atom supercell are shown in Fig. 4(a). Figure 4(b) shows the long-range interaction of $Mn_{Mo}$ defects through the Se 4$p$ states in the spin polarized isosurface plot obtained for two $Mn_{Mo}$ defects separated by a distance of $\sim$6.5 Å in $MoSe_2$. The FM interaction of local moments through delocalized carriers is commonly known as Zener carrier-mediated exchange[19,20] and has also been reported experimentally and theoretically as one of the competing mechanisms for FM ordering in the commonly studied (Ga,Mn)As DMS.[21,22] Among the three compounds, we find Mn substitution in $MoSe_2$ leads to a greater stability of

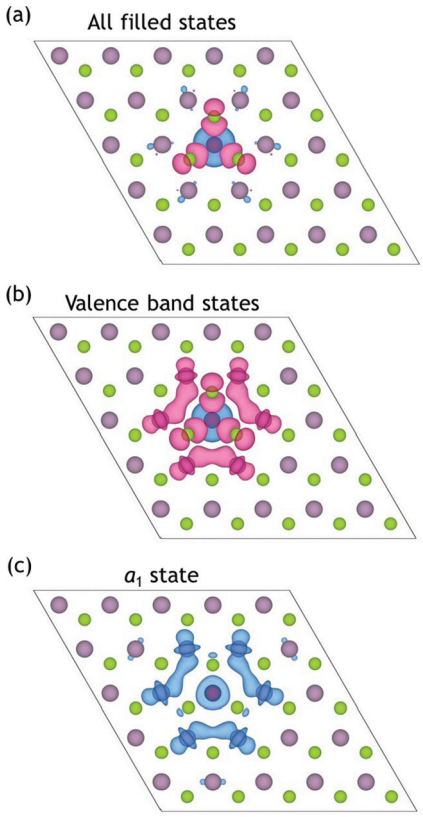


FIG. 3. (Color online) Isosurface plots showing the spin charge density around a $Mn_{Mo}$ defect within a 75 atoms supercell of $MoSe_2$, obtained by (a) integrating over all occupied states, (b) valence band states ranging from $-6.5$ to $-0.8$ eV in Figure 2(a), and (c) the occupied $a_1$ defect state lying within $-0.2$ to 0 eV in Figure 2(a). The isosurface value was taken at 0.001 e/Å$^3$.

FM ordering for nearest-neighbor separation, beyond which, the energy gain with FM ordering becomes comparable for the three compounds. We therefore predict (Mo,Mn)$X_2$ to be strong candidates for 2D DMS. Additionally, we also find FM ordering to be stable on including correlation effects on the Mn 3$d$ states using the DFT + $U$ method[23] for $U$ values ranging from 0 to 5 eV (Supplemental Material Table S2).[16]

The presence of a strong $p$-$d$ exchange interaction in (Mo, Mn)$X_2$, as shown here with a systematic variation of $Mn_{Mo} - Mn_{Mo}$ distances for large supercells ($\geqslant$75 atoms), is in contrast to a recent report by Cheng *et al.*,[9] where the authors observed a very weak gain in energy (of only 0.02 meV) with FM ordering of $Mn_{Mo}$ spins for small supercells (45 atoms). Cheng *et al.*, therefore, suggested a weak Curie temperature ($T_C$) by using a disordered Ruderman-Kittel-Kasuya-Yosida (RKKY) lattice field model.[24] Interestingly, however, they also found a strong energy gain for FM ordering within a 75-atom supercell, which is similar to the present results.

The strength of magnetic interactions between Mn atoms in $MoS_2$, as obtained from our calculations, is similar to that published in another recent report by Ramasubramaniam and Naveh in Ref. 10 (which appeared during the review process of this manuscript), where the authors also note AFM coupling between Mn spins and neighboring S spins. The authors in Ref. 10 have postulated the FM coupling of $Mn_{Mo}$ spins to

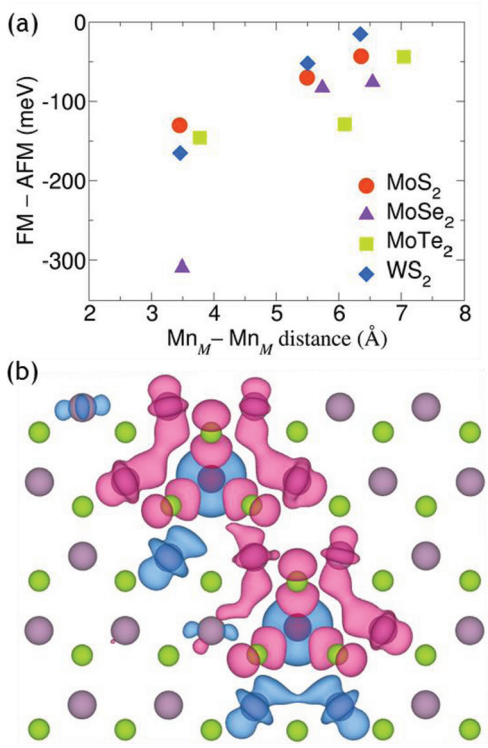


FIG. 4. (Color online) (a) The gain in energy with FM ordering over AFM ordering of spins on two $Mn_{(Mo,W)}$ defects within a 75-atom supercell as a function of the separation between the two defects. A negative energy corresponds to FM ordering being more stable. (b) Isosurface plot showing the spin density when the $Mn_{Mo} - Mn_{Mo}$ defects in $MoSe_2$ are separated by ~6.5 Å. The isosurface value was taken at 0.001 e/Å$^3$.

be governed by double-exchange interactions, which requires the presence of delocalized carriers that can hop between the localized spins and lower the kinetic energy of the system by aligning the localized spins ferromagnetically.[25,26] Thus, the double-exchange mechanism needs delocalized carriers belonging to the chalcogenides $p$ states to be ferromagnetically aligned to the Mn spins, in contradiction to the DFT results obtained in this study.

Given the strong FM interaction between the $Mn_{Mo}$ defects, a natural question that arises is whether other TM elements would also show long-range FM coupling when introduced in the 2D MoDCs? To answer the question, we calculated the energy difference between FM and AFM coupling for pairs of $Fe_{Mo}$, $Co_{Mo}$, and $Ni_{Mo}$ defects in $MoS_2$, $MoSe_2$, and $MoTe_2$. We find that although the interaction between the nearest-neighbor defects is FM, it becomes weakly AFM when the distance between defects increases (see Supplemental Material Fig. S3).[16] In order to understand the difference in the behavior of Mn and the behavior of Fe, Co, and Ni, we take another look at the DOS of $Mn_{Mo}$, and the nearest Mo and Se atoms shown in Fig. 2(b). If we take the difference between the up-spin and down-spin states integrated within the valence band ranging from $-8.5$ to $-2.5$ eV (i.e., excluding the $Mn_{Mo}$ $a_1^{\uparrow}$ state), we get a total magnetic moment of $+1.09$ $\mu_B$ for the $Mn_{Mo}$ defect, $-0.22$ $\mu_B$ for the six nearest Mo atoms, and $-0.25$ $\mu_B$ for the six nearest Se atoms. However, if the integration of the difference between spin channels is only carried out over the occupied $a_1^{\uparrow}$ state, we find a total magnetic moment of $+0.18$ $\mu_B$ for the $Mn_{Mo}$ defect, $+0.22$ $\mu_B$ for the six nearest Mo atoms, and $+0.06$ $\mu_B$ for the nearest Se atoms.

The above result indicates that the coupling between the $Mn_{Mo}$ spins and its neighboring Mo and Se spins, due to the $Mn_{Mo}$ defect state ($a_1^{\uparrow}$), is FM in nature,[27] in contrast to the AFM coupling due to their respective valence band states. Thus, there is a competition between the magnetism arising from the valence band states and the defect states. For the case of Mn substitution, the overall coupling between the $Mn_{Mo}$ spins and its neighboring Se and Mo spins is AFM because only $1e$ is shared between the Mn, Se, and Mo antibonding states. For the case of other TM elements like Fe, Co, and Ni, as the localized TM antibonding states $e_1$ and $e_2$ [Fig. 2(c)] get populated, the overall coupling between the $TM_{Mo}$ spins and the spins on their neighboring Mo and Se atoms becomes FM in nature. The predominantly localized nature of $e_1$ and $e_2$ states results in FM coupling for nearest-neighbor TM defects, but it becomes very weak (even slightly AFM) for TM defects with larger separations.

To further verify the validity of this mechanism, we studied the magnetic ordering with Mn substitution in another 2D dichalcogenide: $WS_2$. As tungsten lies directly below molybdenum in the Periodic Table, $WS_2$ has a similar electronic structure as the other MoDCs, discussed above. A single $Mn_W$ defect in $WS_2$ [with $E_f(Mn_W) = -1.7$ eV], gives rise to an electronic configuration with localized defect states within the band gap, of which, only the Mn $a_1^{\uparrow}$ state is occupied (Supplemental Material Fig. S2).[16] The calculations also show that there is an AFM $p$-$d$ exchange interaction between the $Mn_W$ spin (moment $+0.96$ $\mu_B$) and the neighboring S spins ($-0.01$ $\mu_B$ per S ion). As a consequence, and similar to Mn-doped $MoX_2$, there is a long-range FM ordering of between $Mn_W$ spins, as can be seen from the calculated (FM - AFM) energies shown in Fig. 4(a).

In conclusion, we find the presence of long-range FM ordering between spins of Mn atoms substituted at Mo sites in $MoS_2$, $MoSe_2$, $MoTe_2$ mononlayers, and W sites in $WS_2$ monolayers, respectively. We attribute the microscopic origin for their FM ordering to exchange interactions between the localized Mn spins and the delocalized $p$ spins of chalcogen atoms, which is AFM in nature. Given that FM ordering is found to be robust in four different chalcogenides suggests that it should also be possible to obtain magnetic ordering in other 2D metal dichalcogenides and thus achieve 2D DMS with different band gaps and mobilities. It should also be possible to tune the magnetism in such materials by populating or depopulating the occupied defect states, which are highly localized, as we find here that removing the extra electron in the $a_1^{\uparrow}$ state makes (Mo, Mn)$X_2$ nonmagnetic.

This research was supported by the Materials Sciences and Engineering Division, Office of Basic Energy Sciences (BES), US Department of Energy (DOE) (R.M., S.J.P., S.T.P.), by a Wigner Fellowship through the Laboratory Directed Research and Development Program of Oak Ridge National Laboratory, managed by UT-Battelle, LLC, for the US DOE (WZ), by Oak Ridge National Laboratory's

Shared Research Equipment (ShaRE) User Facility Program (JCI), which is also sponsored by BES US DOE. This research used resources of the National Energy Research Scientific Computing Center, which is supported by the Office of Science of the US DOE under Contract No. DE-AC02-05CH11231.

*Corresponding author: rohan.mishra@vanderbilt.edu

[1]H. Ohno, A. Shen, F. Matsukura, A. Oiwa, A. Endo, S. Katsumoto, and Y. Iye, Appl. Phys. Lett. **69**, 363 (1996).
[2]T. Dietl, Nat. Mater. **9**, 965 (2010).
[3]P. Seneor, B. Dlubak, M.-B. Martin, A. Anane, H. Jaffres, and A. Fert, MRS Bull. **37**, 1245 (2012).
[4]Y. Ma, P. O. Lehtinen, A. S. Foster, and R. M. Nieminen, New J. Phys. **6**, 68 (2004).
[5]S. T. Pantelides, Y. Puzyrev, L. Tsetseris, and B. Wang, MRS Bull. **37**, 1187 (2012).
[6]B. Radisavljevic, A. Radenovic, J. Brivio, V. Giacometti, and A. Kis, Nat. Nanotechnol. **6**, 147 (2011).
[7]Q. H. Wang, K. Kalantar-Zadeh, A. Kis, J. N. Coleman, and M. S. Strano, Nat. Nanotechnol. **7**, 699 (2012).
[8]T. Cao, G. Wang, W. Han, H. Ye, C. Zhu, J. Shi, Q. Niu, P. Tan, E. Wang, B. Liu, and J. Feng, Nat. Commun. **3**, 887 (2012).
[9]Y. C. Cheng, Z. Y. Zhu, W. B. Mi, Z. B. Guo, and U. Schwingenschlögl, Phys. Rev. B **87**, 100401 (2013).
[10]A. Ramasubramaniam and D. Naveh, Phys. Rev. B **87**, 195201 (2013).
[11]P. E. Blöchl, Phys. Rev. B **50**, 17953 (1994).
[12]G. Kresse and J. Hafner, Phys. Rev. B **47**, 558 (1993).
[13]G. Kresse and J. Hafner, Phys. Rev. B **49**, 14251 (1994).
[14]J. P. Perdew, K. Burke, and M. Ernzerhof, Phys. Rev. Lett. **77**, 3865 (1996).
[15]H. J. Monkhorst and J. D. Pack, Phys. Rev. B **13**, 5188 (1976).
[16]See Supplemental Material at http://link.aps.org/supplemental/10.1103/PhysRevB.88.144409 for details of the first-principles calculations.
[17]S. B. Zhang and J. E. Northrup, Phys. Rev. Lett. **67**, 2339 (1991).
[18]F. L. Deepak, R. Esparza, B. Borges, X. Lopez-Lozano, and M. Jose-Yacaman, ACS Catal. **1**, 537 (2011).
[19]C. Zener, Phys. Rev. **81**, 440 (1951).
[20]C. Zener, Phys. Rev. **83**, 299 (1951).
[21]M. Dobrowolska, K. Tivakornsasithorn, X. Liu, J. K. Furdyna, M. Berciu, K. M. Yu, and W. Walukiewicz, Nat. Mater. **11**, 444 (2012).
[22]S. Sanvito, P. Ordejón, and N. A. Hill, Phys. Rev. B **63**, 165206 (2001).
[23]S. L. Dudarev, G. A. Botton, S. Y. Savrasov, C. J. Humphreys, and A. P. Sutton, Phys. Rev. B **57**, 1505 (1998).
[24]D. J. Priour, E. H. Hwang, and S. Das Sarma, Phys. Rev. Lett. **95**, 037201 (2005).
[25]C. Zener, Phys. Rev. **82**, 403 (1951).
[26]P. Mahadevan, A. Zunger, and D. D. Sarma, Phys. Rev. Lett. **93**, 177201 (2004).
[27]We attribute the FM coupling between the $Mn_{Mo}$ spins and the spin on its neighboring Mo atoms, due to the $a_1^{\uparrow}$ state, to superexchange interactions, wherein a $Mn_{Mo}$–Se–Mo bond angle of 84.03° would be expected to be FM, as governed by the Goodenough-Kanamori rules. See, J. Goodenough, Phys. Rev. **100**, 564 (1955); J. Kanamori, J. Phys. Chem. Solids **10**, 87 (1959).